Oral Oncology 95 (2019) 1–10

Contents lists available at ScienceDirect

Oral Oncology

journal homepage: www.elsevier.com/locate/oraloncology

Intracellular calprotectin (S100A8/A9) controls epithelial differentiation and caspase-mediated cleavage of EGFR in head and neck squamous cell carcinoma

Prokopios P. Argyris[a], Zachary Slama[a], Chris Malz[a], Ioannis G. Koutlas[b], Betty Pakzad[c], Ketan Patel[d], Deepak Kademani[d], Ali Khammanivong[e,f], Mark C. Herzberg[a,*]

[a] Department of Diagnostic and Biological Sciences, School of Dentistry, University of Minnesota, Minneapolis, MN 55455, USA
[b] Division of Oral and Maxillofacial Pathology, School of Dentistry, University of Minnesota, Minneapolis, MN 55455, USA
[c] Anatomic Clinical Pathology, North Memorial Health Hospital, Minneapolis, MN 55422, USA
[d] Oral and Maxillofacial Surgery Clinic, North Memorial Health Hospital, Minneapolis, MN 55422, USA
[e] Department of Veterinary Clinical Sciences, University of Minnesota, St. Paul, MN, USA
[f] Masonic Cancer Center, University of Minnesota, Minneapolis, MN 55455, USA

ARTICLE INFO

Keywords:
S100A8/A9
Calprotectin
Premalignant epithelial dysplasia
Head and neck squamous cell carcinoma
P16+ squamous cell carcinoma
Epithelial differentiation
Caspase-3/7
EGFR
VEGF-A
VEGF-C
NGF

ABSTRACT

Objectives: Calprotectin (S100A8/A9) appears to function as a tumor suppressor in head and neck squamous cell carcinoma (HNSCC) and expression in the carcinoma cells and patient survival rates are directly related. We seek to characterize the suppressive role of calprotectin in HNSCC.

Aims: (1) Investigate changes in S100A8/A9 expression as oral carcinogenesis progresses and (2) determine whether intracellular calprotectin can regulate epidermal growth factor receptor (EGFR), a negative prognostic factor, in HNSCC.

Materials and methods: Using immunohistochemistry (IHC), S100A8/A9 was analyzed in HNSCC specimens (N = 46), including well-differentiated (WD, N = 19), moderately-differentiated (MD, N = 14), poorly-differentiated (PD, N = 5) and non-keratinizing/basaloid (NK/BAS, N = 8), and premalignant epithelial dysplasias (PED, N = 16). Similarly, EGFR was analyzed in HNSCCs (N = 21). To determine whether calprotectin and EGFR expression are mechanistically linked, TR146 HNSCC cells that are S100A8/A9-expressing or silenced (shRNA) were compared for EGFR levels and caspase-3/7 activity using western blotting and immunofluorescence microscopy.

Results: In normal oral mucosal epithelium, S100A8/A9 stained strongly in the cytoplasm and nucleus of suprabasal cells; basal cells were consistently S100A8/A9 negative. In PED and HNSCC, S100A8/A9 expression was lower than in adjacent normal epithelial tissues (NAT) and declined progressively in WD, MD, PD and NK/BAS HNSCCs. S100A8/A9 and EGFR levels appeared inversely related, which was simulated *in vitro* when S100A8/A9 was silenced in TR146 cells. Silencing S100A8/A9 significantly reduced caspase-3/7 activity, whereas EGFR levels increased.

Conclusions: In HNSCC, S100A8/A9 is directly associated with cellular differentiation and appears to promote caspase-3/7-mediated cleavage of EGFR, which could explain why patients with S100A8/A9-high tumors survive longer.

Introduction

Head and neck squamous cell carcinomas (HNSCC) represent the sixth most prevalent human malignancy worldwide and are characterized by high mortality and morbidity [1,2]. Etiological factors can include tobacco metabolites, alcohol consumption, and human papillomavirus (HPV) infection [3,4]. The overall five-year survival rate for HNSCC patients remains 50–66% despite improved therapeutic interventions [5,6].

In humans, S100A8 and S100A9 typically form heterodimers (S100A8/A9), while homodimers are not normally detectable [7]. Monomers and homo-trimeric or -tetrameric complexes are also

* Corresponding author at: University of Minnesota, 17-164 Moos Tower, 515 Delaware St. SE, Minneapolis, MN 55455, USA.
E-mail address: mcherzb@umn.edu (M.C. Herzberg).

https://doi.org/10.1016/j.oraloncology.2019.05.027
Received 27 November 2018; Received in revised form 21 May 2019; Accepted 29 May 2019
Available online 04 June 2019
1368-8375/

possible but less frequent [8]. Calprotectin, the heterodimeric complex of S100A8 and S100A9, appears to be a tumor-suppressor in HNSCC [9–11] and reduction in protein expression is associated with poor patient outcomes [10,12]. A member of the S100 superfamily of EF-hand calcium-binding proteins [10,13,14], calprotectin is constitutively expressed in the cytoplasm of squamous epithelial cells lining the oral, oropharyngeal and genitourinary mucosae [11,15]. Encoded by the epidermal differentiation complex (EDC) on chromosome 1q21, intraepithelial S100A8/A9 appears to contribute to epithelial differentiation and growth [16], and control proliferation, cell cycle progression and growth of carcinoma cells through activation of the G2/M DNA damage checkpoint [9,11]. Silencing expression of S100A8 and S100A9 in HNSCC cells enhances MMP-2 activity, cell invasion and migration *in vitro* [17]. In HNSCC patients, calprotectin expression in tumor cells and overall survival are directly related and associated with levels of DNA methylation [10].

Considered a negative prognostic indicator, epidermal growth factor receptor (EGFR or ERBB1/HER1) is overexpressed in approximately 80–90% of HNSCCs [18,19]; variability in cell surface EGFR may reflect cleavage by caspases 1, 3 and 7 [20,21]. Furthermore, neuronal and carcinoma cells release nerve growth factor (NGF) [22], which is linked to perineural invasion and metastasis in malignancies including HNSCC [23,24], whereas vascular endothelial growth factor -A (VEGF-A) and -C (VEGF-C) drive tumor vascularization [25,26] and contribute to lymph node metastasis [27,28]. How calprotectin within tumor cells associates with key prognostic markers is not known.

We seek to understand why patient outcomes are better in calprotectin-high than -low HNSCC tumors. We hypothesized that loss of S100A8/A9 affects the expression of tumor-promoting proteins EGFR, NGF and/or VEGF-A/-C. Our data strongly suggest that calprotectin expression positively associates with differentiation of malignant epithelial cells (grading) in primary HNSCC tumors. RNA sequencing (RNA-seq) analysis of data from The Cancer Genome Atlas (TCGA) project (http://cancergenome.nih.gov) shows that caspases 1, 3, 7, and 8 expression strongly correlates with S100A8 and S100A9 in HNSCC. Loss of S100A8/A9 abolishes caspases 3/7 activity and apoptotic cell death, and inversely correlates with EGFR protein expression *in vitro* and *ex vivo*. These findings could explain why patients with S100A8/A9-high tumors survive longer.

Materials and methods

Stable knockdown of S100A8/A9 in a human HNSCC cell line

Using TR146 cells, a well-differentiated buccal carcinoma cell line, endogenous S100A8/A9 expression was silenced using an shRNA expression vector (TR146-shRNA-S100A8/A9-KD) as previously described [9,29]. An expression vector containing scrambled shRNA was used as a negative control (TR146-shRNA-control). Knockdown of S100A8 and S100A9 protein expression was confirmed and quantified using Western blotting and normalized against β-actin levels.

Cell culture conditions

TR146 cells were maintained in Dulbecco's Modified Eagle's Medium/Ham's F-12 (DMEM/F-12; 1:1 vol ratio) supplemented with 10% fetal bovine serum (complete medium) in 5% CO_2 at 37 °C. TR146-S100A8/A9-KD and TR146-shRNA-control cells were cultured in complete medium supplemented with 250 μg/ml G418 sulfate (Corning, Corning, NY USA) serving as a selection marker. Before assays, cells were preconditioned (> 24-h) in complete medium without G418 sulfate.

TERT-2/OKF-6 (BWH Cell Culture and Microscopy Core, Boston, MA, USA) cells are immortalized, S100A8/A9-expressing, non-neoplastic oral keratinocytes of the floor of the mouth [30–32]. TERT-2/OKF-6 cells were cultured in 5% CO_2 at 37 °C in defined serum-free keratinocyte medium (1 × K-SFM) supplemented with EGF and bovine pituitary extract (BPE) (Thermo Fischer Scientific, Waltham, MA USA).

Caspase-3/7 activity assay

TR146, TR146-S100A8/A9-KD and TR146-control (3.2×10^5 cells each) were allowed to adhere to glass coverslips and cultured in 12-well plates for 24 h. Adherent cells were then exposed to 5-Gy of X-radiation, an optimized dose that induced maximum levels of apoptosis. After irradiation, cells from each TR146 line were harvested at 30 min, 3 h, and 24 h and assayed for caspase-3/7 activity using the Magic Red® Caspase-3/7 Assay Kit (#936, Bio-Rad, Hercules, CA USA) following the manufacturer's instructions. Nuclei were highlighted using Hoechst staining. Cells from each line were visualized using an upright fluorescence microscope (Nikon Eclipse E800) and images were captured at each time point from at least 4 different fields at 20× magnification via SPOT Advanced Software (Spot Imaging, Sterling Heights, MI USA) under consistent gamma, brightness, and exposure time settings. Immunofluorescence density was quantified using ImageJ software (https://imagej.nih.gov).

EGFR and VEGF-A immunofluorescent staining in TR146 cells

The TR146 cell lines (1×10^5 cells each) were seeded and allowed to adhere to glass coverslips for 24 h. Adherent cells were then rinsed with phosphate-buffered saline (PBS) and fixed in ice-cold methanol for 15-min at room temperature (RT) for immunofluorescent (IF) staining. To block non-specific binding of primary antibodies, cells were incubated for 30 min in 1% bovine serum albumin (BSA; #A7906, Sigma-Aldrich, St. Louis, MO USA) in PBS with 0.1% Tween-20 (PBS-T). Following the blocking step, rabbit anti-human EGFR (EP38Y, ab52894, Abcam, Cambridge, MA USA) and mouse anti-human VEGF-A (VG-1, ab1316, Abcam) antibodies were diluted 1:100 in 1% BSA in PBS-T (1% BSA/PBS-T) and incubated on cells for 1 h in a humidified chamber. Cells were then washed 3× with PBS for 5-min each and incubation was continued for another 60 min in the dark with Alexa Fluor 488-conjugated goat anti-rabbit IgG (H + L) (Thermo Fisher Scientific, #A32731) and Alexa Fluor 568-conjugated goat anti-mouse IgG (H + L) (Thermo Fisher Scientific, #A-11036) secondary antibodies diluted 1:500 in 1% BSA/PBS-T. To stain for nuclei, cells were incubated for 5 min with DAPI (4′,6-diamidino-2-phenylindole dihydrochloride; Sigma-Aldrich, # D9542), air dried for 20 min in the dark, mounted on glass slides using Fluoromount-G mounting medium (eBioscience, Thermo Fisher Scientific), and visualized by fluorescence microscopy as above. Isotype antibody was used as a negative control. Immunofluorescence density was quantified using ImageJ software from at least 3 different fields for each cell line at 20× magnification.

Western blot analysis

Cells were harvested at 70–80% confluency, washed twice with 1–2 ml ice-cold (~4°C) Dulbecco's-PBS, lysed in standard radioimmunoprecipitation assay (RIPA) buffer with protease inhibitors, centrifuged at 4 °C at 21,000*g* for 5 min, and soluble protein concentrations were measured using the Bicinchoninic Acid assay. Samples were boiled for 10 min in 1 × sample buffer (1% SDS in 31.25 mM Tris-HCl, pH 6.8 with 12.5% glycerol, 0.005% bromophenol blue, and 2.5% beta-mercaptoethanol), loaded onto SDS-polyacrylamide gels at 50–100 μg total protein per well, separated at 120 V for approximately 80 min, and then transferred onto nitrocellulose membranes using a Bio-Rad semi-dry protein transfer apparatus. Membranes were blocked for 1 h at RT using Odyssey Blocking Buffer (LI-COR Biosciences, Lincoln, NE USA) diluted 1:1 in PBS (without Tween-20), incubated overnight at 4 °C with primary antibodies in Odyssey Blocking Buffer supplemented with 0.1% Tween-20 at indicated dilution ratios: Anti-human S100A8 (Calgranulin A, C-10, sc-48352, Santa Cruz

Biotechnology), 1:40; anti-S100A9 (Calgranulin B, H-90, sc-20173, Santa Cruz Biotechnology), 1:100; anti-EGFR (EP38Y, ab52894, Abcam), 1:1000; anti-VEGF-A (VG-1, ab1316, Abcam), 1:1000; anti-VEGF-C (PA5-29772, Thermo Fisher Scientific), 1:1000; and anti-NGF (EPI320Y, Abcam, ab52918), 1:500. Mouse anti-β-actin (sc-47778, Santa Cruz Biotechnology) at 1:500 dilution served as protein loading control. Membranes were next incubated for 1 h in LI-COR IRDye 800CW goat anti-rabbit (#926-32211) and LI-COR IRDye 680RD goat anti-mouse (#926-68070) secondary antibodies at 1:5000 dilution. Antigens were visualized using a LI-COR Odyssey infrared imaging system.

Immunohistochemistry (IHC)

All tissues were obtained using a North Memorial Medical Center Institutional Review Board approved protocol. All formalin-fixed, paraffin-embedded (FFPE) specimens were derived from incisional or excisional intraoral biopsies from patients with precancerous or carcinomatous lesions. HNSCC tumor cases (N = 46) were classified using the 2017 WHO Classification of Head and Neck Tumors: Well-differentiated (WD, N = 19); moderately differentiated (MD, N = 14); and poorly differentiated (PD, N = 5). Non-keratinizing/basaloid HNSCCs (NK/BAS, N = 8) showing limited or absent squamous epithelial differentiation were included. Premalignant epithelial dysplasias (PED, N = 16) were graded as mild, moderate and severe. For each lesion, the age and gender of the patient, location, clinical stage (TNM), and p16 status were noted (Supplementary Tables 1, 2, and 3).

Tissues were sectioned at 4 μm, mounted on adhesive slides, dried (7 min, 65 °C), deparaffinized (5 min twice in CitrisolvTM; Decon Labs, #1601), then rehydrated in graded alcohol (3 min each at 100%, 95%, and 70%), and rinsed in water. Epitopes were retrieved by incubating the slides in 1× Retrieve-All Antigen Unmasking System 2: Basic (BioLegend, San Diego, CA USA) at 65°C for 1 h, followed by a 10-min "cool-down" in RT. Slides were then placed in 3% H_2O_2 in PBS for 5 min at RT to quench endogenous peroxidase activity. Non-specific binding was blocked with 1% BSA/TBS-T for 1 h at RT and serial sections of each tumor were immersed completely in primary antibodies for 1 h at RT and rinsed 3× with TBS. Isotype antibodies were used as negative controls. Slides were then immersed in biotinylated anti-mouse or anti-rabbit secondary antibody (1:500 in 1% BSA/TBST) for 1 h, RT (antibodies as listed, Supplementary Tables 4, 5), followed by streptavidin-HRP (30-min, RT; eBioscience, #18–4100-94; 1:250 in blocking buffer). Peroxidase product was developed using the Vector-Nova Red peroxidase substrate kit (7–10 min, RT; Vector laboratories, # SK-4800), rinsed in tap water, counterstained in hematoxylin (< 5 min), dehydrated in graded alcohol and CitrisolvTM, and cover-slipped.

IHC scoring system and statistical analysis

S100A8, S100A9 and EGFR immunopositivity was semi-quantified as previously reported [12]. Stained lesional cells per 10x-magnification field were scored 1 = 0% positive cells, 2 = < 33%, 3 = 34–66%, and 4 = > 66% positive cells, whereas immunostain intensity was scored 1 = no staining, 2 = weak, 3 = moderate, and 4 = strong). For each specimen, the expression score (the % of stained cells × intensity, range 1–16) for intracellular localization and staining distribution were also recorded. For S100A8/A9 and EGFR staining, lesions were classified as high (≥9) or low (< 9) expression score.

Normality of the data distribution for each group of lesions was assessed using the Shapiro-Wilks test. Since some variables showed non-normal distribution, differences in S100A8 and S100A9 expression between groups were determined using non-parametric Kruskal-Wallis one-way ANOVA, whereas EGFR levels in S100A8/A9-high and -low HNSCC were analyzed using the Mann-Whitney *U* test. A p-value < 0.05 indicated a statistically significant difference. For each immunohistochemical marker and group, median and range were reported.

RNA sequencing analysis in S100A8/A9-low and -high HNSCC samples

The HNSCC RNA sequence (level 3 RNA-Seq V2) dataset was downloaded from The Cancer Genome Atlas (TCGA) database (http://cancergenome.nih.gov) and analyzed for mRNA expression. The expression data from 521 HNSCC tumors were processed and analyzed as previously described [10]. Total sequencing reads per million (RPM) for each transcript was calculated and normalized to the housekeeping gene glyceraldehyde-3-phosphate dehydrogenase (GAPDH). HNSCC patients were then stratified into two extreme groups based on S100A8 and S100A9 expression levels to represent S100A8/A9-low (RPM ≤ 100 for both S100A8 and S100A9; n = 89) and S100A8/A9-high (RPM ≥ 1000 for both S100A8 and S100A9; n = 104). The S100A8/A9-low and -high groups were compared for expression of CASP1, CASP3, CASP7, CASP8, EGFR, NGF, VEGF-A/C transcripts using GraphPad Prism (GraphPad Software, Inc., San Diego, CA USA). Statistical analysis was performed using unpaired two-tailed Student's *t-test* with equal variance. For RNAseq data, the mean ± SEM for each patient group was reported.

Results

Differentiation and progression of head and neck carcinogenesis: S100A8/A9 expression

Using immunohistochemistry, S100A8 and S100A9 protein levels were compared in non-neoplastic (normal) adjacent mucosal epithelial tissues (NAT) and mild, moderate, and severe PED (Fig. 1A). S100A8 and S100A9 immunostaining was strong and diffuse in the nucleus and cytoplasm of the NAT, whereas the basal cell layers were consistently negative. Unlike the NAT, PED showed focal S100A8/A9 loss and weaker staining within the dysplastic areas of the spinous cell layer (black arrows). PED cases (6 mild, 9 moderate and 1 severe) located typically at the lateral and ventral tongue (68.8%) and distributed equally between men and women (M:F = 1:1). The mean age at diagnosis was 60.9 ± 12.3 years (median = 59, range = 44–77) (Table 1, Supplementary Table 1).

Invasive HNSCC cases were classified as WD, PD, and NK/BAS (Fig. 1B). Phenotypically resembling stratified squamous epithelium, WD HNSCC showed strong, diffuse S100A8 and S100A9 immunostaining. In most PD neoplastic cells, atypia and nuclear pleomorphism were associated with lost S100A8/A9 expression, whereas basal epithelial cell-like NK/BAS HNSCC was consistently S100A8/A9-negative (Fig. 1B). These lesions occurred most frequently on the lateral and ventral surfaces of the tongue (58.7%) and palate (10.9%); 29 (63%) were from males and 17 (37%) from females (M:F = 1.7:1); mean age at diagnosis was 60.8 years ± 15.7 (median = 61.5, range = 24–95). Of the 46 HNSCC cases, 6 (13%) were p16 positive (p16+) and 11 (23.9%) presented with confirmed cervical lymph node involvement (Table 1, Supplementary Table 2).

Immunoreactive S100A8/A9 expression was similar in NAT and WD HNSCC. When compared to NAT, S100A8/A9 was decreased in PEDs and was significantly less in HNSCCs [MD ($p < 0.01$), PD ($p < 0.001$), NK/BAS ($p < 0.0001$)] (Fig. 1C, D). S100A8/A9 decreased progressively from WD to MD ($p < 0.01$) to PD ($p < 0.01$) to basaloid carcinomas ($p < 0.0001$) lacking keratinization (NK/BAS HNSCC). In HNSCC, therefore, S100A8/A9 expression positively correlated with squamous differentiation (Supplementary Table 2).

To characterize calprotectin in metastatic lesions, 11 HNSCC primary tumors and paired lymph node metastases were immunostained for S100A8 and S100A9. S100A8 and S100A9 were expressed in WD but not in PD metastatic carcinoma cells (Supplementary Table 3 and Supplementary Fig. A). In general, calprotectin levels tended to be lower ($p > 0.05$) in metastatic tumors from cervical lymph nodes than

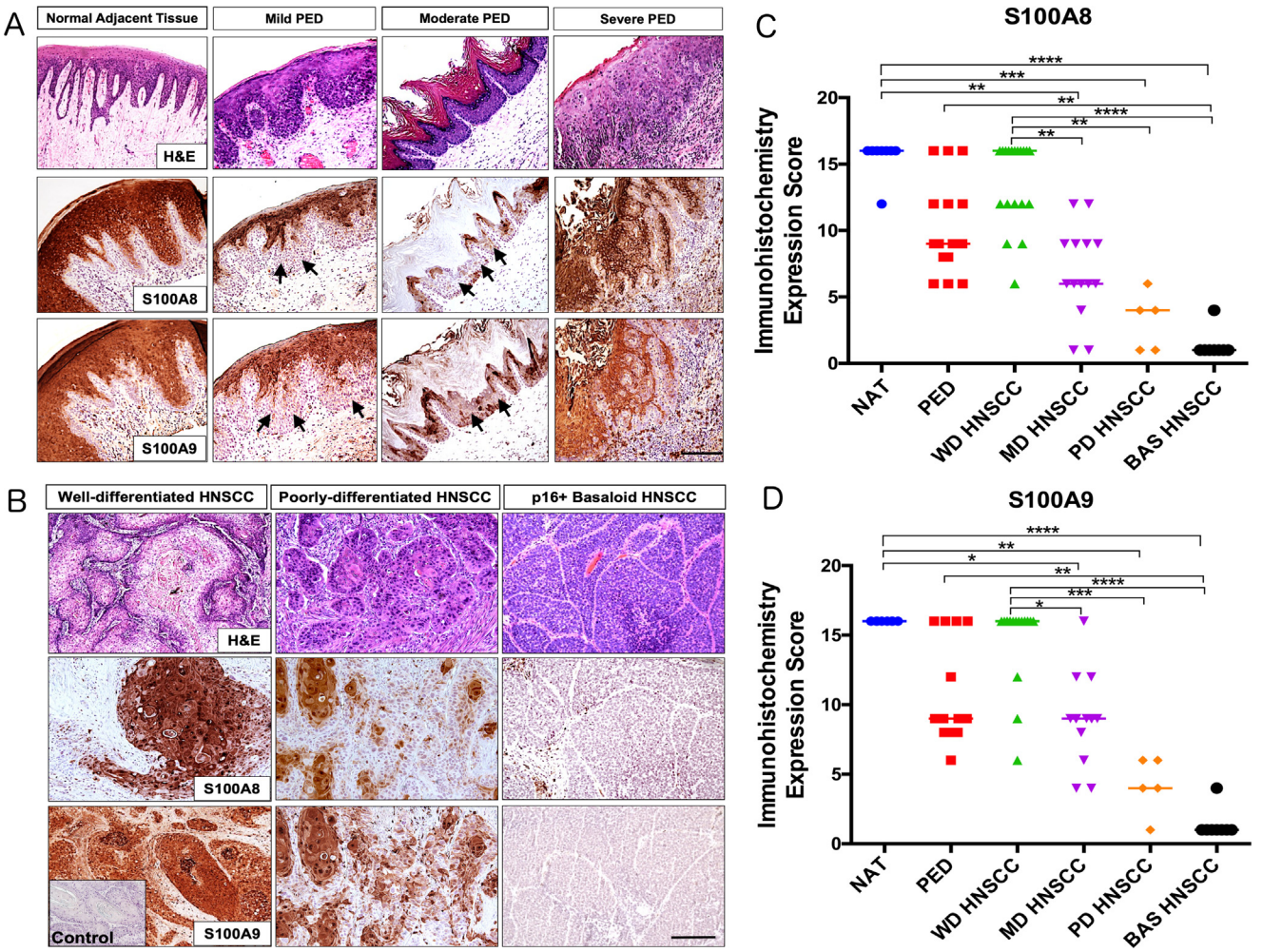

Fig. 1. S100A8/A9 expression during differentiation and progression of head and neck carcinogenesis. (A) Histopathologic and S100A8/A9 immunohistochemical features of normal mucosal epithelium and premalignant epithelial dysplasias (PED). S100A8 and S100A9 subunits of the calprotectin complex were diffusely and strongly expressed in the stratified squamous oral epithelium except for the basal cell layer. Foci of lost S100A8 and S100A9 (black arrows) in PED (N = 16); overall, weaker intensity of immunostaining when compared to normal adjacent tissue (NAT) (scale bar = 200 μm). (B) Histopathologic and S100A8/A9 immunohistochemical features of HNSCC. HNSCC specimens (N = 46) were classified as WD (N = 19), MD (N = 14), PD (N = 5), and NK/BAS (N = 8) tumors. Phenotypically resembling oral mucosal epithelia, WD HNSCC showed strong, diffuse S100A8 and S100A9 immunostaining. S100A8/A9 expression was lost in anaplastic PD specimens. Consistently S100A8/A9-negative, p16+ NK/BAS tumors generally lost squamous features (scale bar = 100 μm). The isotype antibody negative control is also shown. Quantification of immunoreactive (C) S100A8 and (D) S100A9 in normal adjacent epithelial tissue (NAT, N = 8), premalignant epithelial dysplasias (PED, N = 16) and head and neck squamous cell carcinomas (HNSCC, N = 46). S100A8 and S100A9 protein levels progressively decreased during the transition from NAT to precancerous lesions. S100A8/A9 approaches complete loss in less differentiated or non-keratinizing/basaloid HNSCC when compared to NAT or well-differentiated tumors (Median, ** $p < 0.01$, *** $p < 0.001$, **** $p < 0.0001$, non-parametric Kruskal-Wallis test).

Table 1
Collective presentation of the clinicopathologic and demographic characteristics of the clinical cases studied.

Specimens	Gender	Age (years)	Location	Histopathologic classification
HNSCC (N = 46)	29 M: 17F	Mean = 60.8 Median = 61.5 Range = 24–95	Lateral and ventral tongue (27, 58.7%) Palate (5, 10.9%) Gingiva (3, 6.5%) Base of tongue (2, 4.3%) Floor of mouth (4, 8.7%) Others (5, 10.9%)	WD (19, 41.3%) MD (14, 30.4%) PD (5, 10.9%) NK/BAS (8, 17.4%) p16 (+): 6/46 (13%)
PED (N = 16)	8 M: 8F	Mean = 60.9 Median = 59 Range = 44–77	Lateral and ventral tongue (11, 68.8%) Floor of mouth (2, 12.5%) Palate (1, 6.2%) Buccal mucosa (1, 6.2%) Retromolar trigone (1, 6.2%)	Mild (6, 37.5%) Moderate (9, 56.3%) Severe (1, 6.2%)

HNSCC, head and neck squamous cell carcinoma; WD, well-differentiated; MD, moderately-differentiated; PD, poorly-differentiated; NK/BAS, Non-keratinizing/basaloid; PED, premalignant epithelial dysplasia.

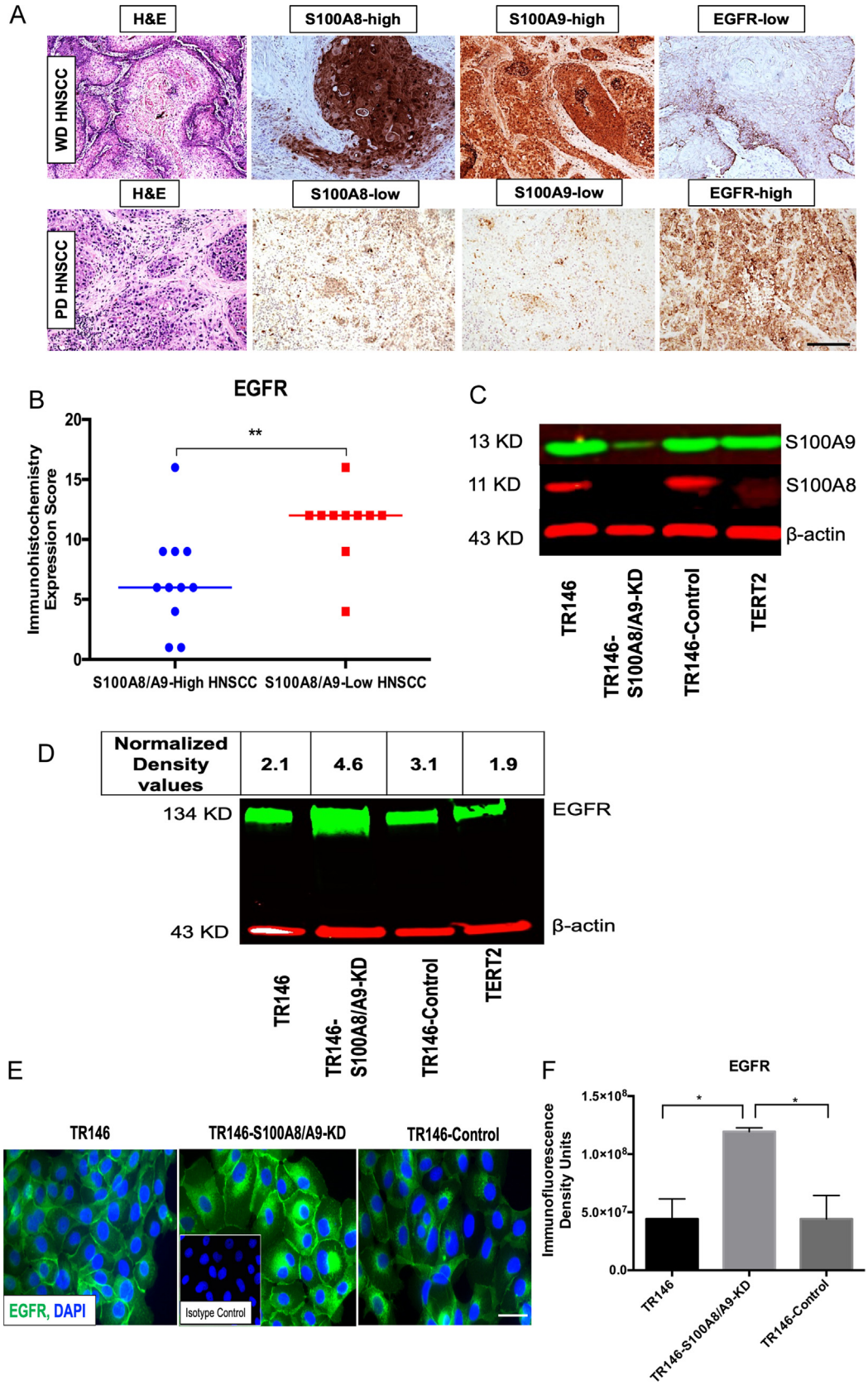

(caption on next page)

Fig. 2. Calprotectin inversely correlates with EGFR expression in HNSCC. (A) EGFR immunoreactivity in S100A8/A9-high (N = 11) and S100A8/A9-low (N = 10) HNSCC. (B) Membrane-associated immunoreactive EGFR was lower in S100A8/A9-high tumors than S100A8/A9-low tumors (scale bar = 100 μm, median, ** $p < 0.01$, Mann-Whitney *U* test). (C) S100A8 (red) and S100A9 (green) in TR146 cells before (TR146 parental cells) and after knockdown using shRNA for S100A8 and S100A9 (TR146-S100A8/A9-KD), TR146-scrambled shRNA-control, and immortalized oral keratinocytes (TERT2). Representative immunoblotting (from at least two independent repeats) is shown. β-actin was used for total protein loading control. (D) Silencing of S100A8/A9 upregulates EGFR protein expression *in vitro*. EGFR (green) in TR146, TR146-S100A8/A9-KD and TR146-shRNA-control, and TERT2 cells. β-actin was used for total protein loading control. Shown is a representative immunoblot from two independent repeats. Calprotectin-expressing TR146, TR146-control and TERT2 cells expressed less EGFR protein than TR146-S100A8/A9-KD. (E) EGFR (green) expression in S100A8/A9-KD relative to the parental and shRNA-control TR146 cells visualized using immunofluorescence microscopy. DAPI (blue) highlighted cell nuclei. S100A8/A9-knockdown TR146-S100A8/A9-KD cells appeared to show greater EGFR levels than S100A8/A9-positive TR146 and TR146-shRNA-control HNSCC cells (representative images from at least three biological replicates, scale bar = 50 μm). The negative isotype control is shown in the insert. (F) Quantification of the immunofluorescence density in TR146, TR146-S100A8/A9-KD and TR146-shRNA-control cells (Mean ± SEM, * $p < 0.05$, One-way Anova Tukey HSD test). (For interpretation of the references to color in this figure legend, the reader is referred to the web version of this article.)

in the corresponding primary HNSCCs (Supplementary Fig. 1B).

Calprotectin and EGFR expression inversely correlated in HNSCC

In HNSCC, WD S100A8/A9-high lesions were marked by low expression of immunoreactive EGFR, whereas PD S100A8/A9-low carcinomas were EGFR-high (membranous and cytoplasmic; $p < 0.01$) (Fig. 2A, B). Silencing S100A8/A9 in TR146 cells (TR146-S100A8/A9-KD) *in vitro* (Fig. 2C) increased immunoreactive EGFR above TR146 wild-type cells, TR146-shRNA-control, or TERT2 immortalized oral keratinocytes (Fig. 2D-F). Hence, S100A8 and S100A9 (calprotectin) expression were inversely related to EGFR levels *in vitro* in a model of well-differentiated HNSCC and *ex vivo*.

Loss of S100A8/A9 dampens post-radiation caspase-3/7 activity

We sought to determine whether changes in EGFR expression reflected calprotectin-dependent caspase activation and subsequent EGFR cleavage [20,21]. TR146 HNSCC cells were X-irradiated over time to activate caspase 3/7. Silencing S100A8/A9 significantly reduced caspase-3/7 activity at 30-min ($p < 0.01$), 3-h ($p < 0.01$) and 24-h ($p < 0.05$) post-radiation (Fig. 3A and B). Next, HNSCC cases were dichotomized into S100A8/A9-high and -low tumors using the TCGA RNA-seq data (Fig. 3C). CASP1 ($p < 0.0001$), CASP3 ($p = 0.0005$), CASP7 ($p < 0.0001$), and CASP8 ($p < 0.001$) expression was significantly higher in S100A8/A9-high than S100A8/A9-low carcinomas (Fig. 3D).

Calprotectin status in HNSCC cases does not affect VEGF-A/C or NGF protein expression

In human HNSCC samples, expression of S100A8/A9 and VEGF-A/-C cytoplasmic immunostaining appeared mutually independent (Supplementary Fig. 2A). VEGF-A distribution and density varied from focal to diffuse and weak to strong, while VEGF-C stained diffusely with weak to moderate intensity in all HNSCC cases. In TR146 HNSCC cells, silencing calprotectin did not appear to affect VEGF-A expression (Supplementary Fig. 2B). VEGF-A/-C protein expression was similar in S100A8/A9-expressing TR146 wild-type, TR146-S100A8/A9-KD, TR146-control, and TERT-2 cells (Supplementary Fig. 2C).

Similarly, NGF expression appeared to be unaffected by calprotectin status in HNSCC (Supplementary Fig. 3). Both S100A8/A9-high and -low HNSCC specimens showed diffuse, weak to strong NGF cytoplasmic immunopositivity (Supplementary Fig. 3A). NGF protein expression appeared unaffected by silencing S100A8/A9 in TR146 cells (Supplementary Fig. 3B).

EGFR, VEGF-A/C and NGF expression in S100A8/A9-high and -low HNSCC: TCGA

We next interrogated TCGA database for differences in EGFR, VEGF-A/C and NGF mRNA expression between tissues from S100A8/A9-high and -low HNSCC human tumors. Using RNA-seq data, angiogenesis-related VEGF-A/C mRNAs were significantly greater ($p < 0.001$) in tumors than NAT; EGFR and NGF mRNA levels appeared similar in NAT and tumors (Fig. 4A). Interestingly, VEGF-A/C and NGF mRNA levels were significantly greater ($p < 0.05$) in S100A8/A9-high than -low HNSCC (Fig. 4B). EGFR mRNA expression was similar in S100A8/A9-high and -low neoplasms (Fig. 4B).

Discussion

Calprotectin suppresses carcinoma cell growth by signaling PP2A-dependent inactivation of the cyclin B1/p-Cdc2 (Thr14/Tyr15) complex to arrest cell cycle at the G2/M checkpoint [9]. Calprotectin also inhibits MMP-2 activity, cell migration and invasion *in vitro* [17]. In patients with HNSCC, aggressive tumor behavior and poor survival are associated with EGFR upregulation [18,19]. EGFR engagement by EGF activates ERK, PI3K/AKT and JAK/STAT signaling pathways, promoting cell proliferation, migration, metastasis, and evasion of apoptosis [18]. Within HNSCC tumor cells, S100A8/A9 and tumor-promoting EGFR protein expression are now shown to be inversely related *in vitro* and *ex vivo*. Whereas S100A8/A9-high HNSCC specimens express significantly less EGFR than S100A8/A9-low tumors, silencing of endogenous S100A8 and S100A9 in TR146 buccal carcinoma cells increases EGFR. Not surprisingly, the inverse relationship between S100A8/A9 and EGFR in tumor cells is masked using data from TCGA, which reports whole tumor tissue mRNA including stromal and tumor-infiltrating lymphoid cells. Hence, S100A8/A9 appears to suppress EGFR-stimulated tumorigenesis *in vivo* in HNSCC [10]. Intracellular S100A8/A9-mediated control of EGFR expression may be a contributory suppressive mechanism in HNSCC.

S100A8/A9-driven EGFR suppression appears to involve post-translational caspase-mediated cleavage of EGFR. S100A8/A9 induces autophagy and apoptosis, and significantly increases caspase-3/7 activity in multiple human cell types, including epithelial cells [33,34]. Notably, caspases 1, 3 and 7 readily cleave EGFR *in vitro* [20,21]. In our study, silencing calprotectin in a buccal carcinoma cell line abolished post-radiation caspase-3/7 activity and increased EGFR surface expression. Conversely, calprotectin-expressing cells showed elevated caspase-3/7 activity and reduced EGFR levels. The S100A8/A9-dependent increase in caspase-3/7 activity appears to drive proteolytic cleavage of EGFR *in vitro*, which would impair EGFR-dependent downstream signaling, including tyrosine phosphorylation of PLC-gamma1, Akt and ERK1/2, as previously reported [20,35]. Furthermore, *CASP1*, *3* and *7* transcripts are significantly greater in S100A8/A9-high than -low tumors. In HNSCC, therefore, S100A8/A9-mediated increases in caspase-3/7 levels and activity, followed by post-translational cleavage of EGFR can negatively regulate surface EGFR (Fig. 5).

During progressive development of HNSCC, S100A8/A9 mRNAs [10,36–38] and the respective proteins decline as we report. Premalignant, dysplastic lesions (PED) of the oral mucosa show significantly lower expression of S100A8 and S100A9 than phenotypically normal oral stratified squamous epithelia. Although some PED specimens appear to maintain high S100A8/A9 levels (expression score ≥ 12; Supplementary Table 4), most PEDs showed loss of

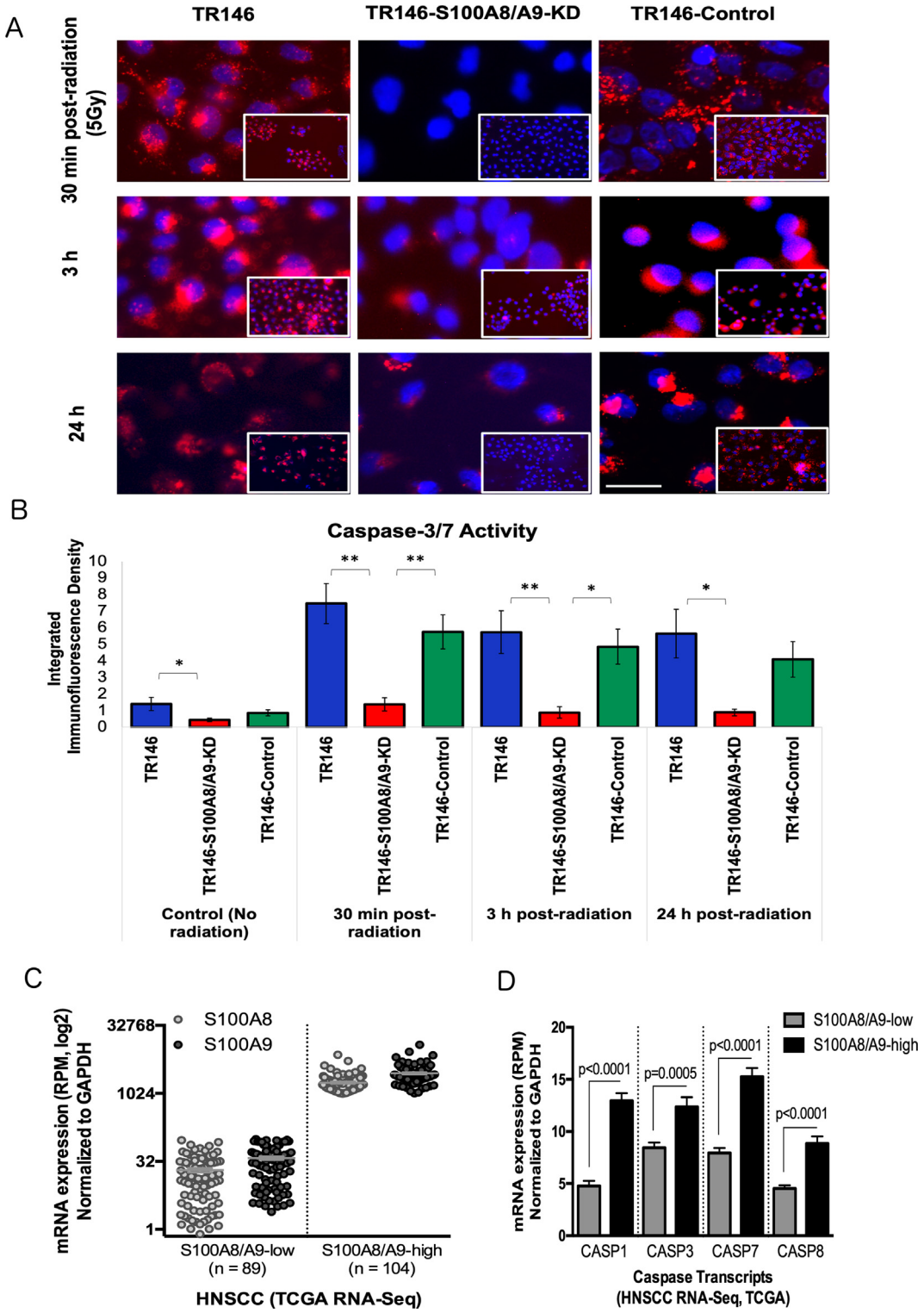

Fig. 3. Loss of S100A8/A9 dampens post-radiation caspase-3/7 apoptotic activity. (A) TR146, TR146-S100A8/A9-KD and TR146-shRNA-control were exposed to 5-Gy of X-radiation to induce caspase-mediated apoptosis. Caspase-3/7 activity was visualized 30-min, 3-h and 24-h after exposure. Radiation-sensitive, calprotectin-expressing, TR146 and TR146-shRNA-control apoptotic cells bear numerous orange-red lysosomal bodies and less intense blue nuclei. TR146-S100A8/A9-KD cells appear less sensitive to X-radiation, however, evade apoptosis and show absent or reduced orange-red lysosomal staining (representative images from three biological replicates, scale bar = 60 μm, insets; low-power images of the corresponding high-power ones). (B) Quantification of activated caspase-3/7 in TR146, TR146-S100A8/A9-KD and TR146-shRNA-control. Over time, X-irradiation activated caspase-3/7 in S100A8/A9-expressing TR146 HNSCC cells, whereas silencing of S100A8/A9 significantly reduced caspase-3/7 activity at 30-min, 3-h and 24-h post-radiation (Mean ± SEM, * $p < 0.05$, ** $p < 0.01$, one-way Anova Tukey HSD test). (C) TCGA cases of HNSCC were separated into two groups and dichotomized into low and high S100A8 and S100A9 cohorts based on weak (reads per million, or RPM ≤ 100 counts) or strong (RPM ≥ 1000 counts) expression levels. (D) *Caspase 1, 3, 7,* and *8* expression in S100A8/A9-low and -high tumor samples: S100A8/A9-high HNSCCs significantly upregulate caspase mRNA levels. Comparative analysis was performed between S100A8/A9-low (n = 89) and -high (n = 104) HNSCC samples (Mean ± SEM, two-tailed Student's *t*-test with equal variance). (For interpretation of the references to color in this figure legend, the reader is referred to the web version of this article.)

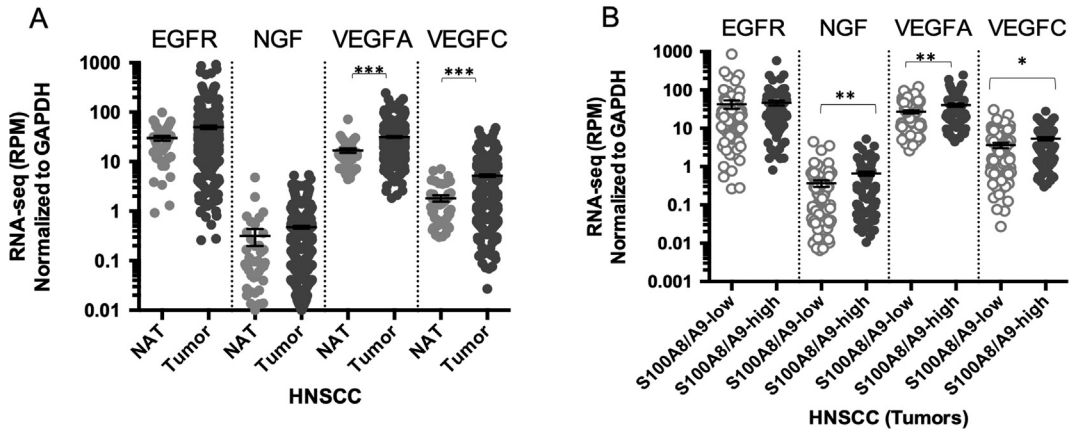

Fig. 4. EGFR, NGF, VEGF–A and VEGF–C in normal and HNSCC samples relative to S100A8 and S100A9. (A) EGFR, NGF, VEGF-A and VEGF-C gene expression (mRNA) profiles in normal adjacent tissues (N = 43) and HNSCC (N = 521) normalized to GAPDH using TCGA RNA-seq data. Expression data shown as Mean ± SEM; ***p = 0.0006 (two-tailed Student's *t*-Test with equal variances). (B) TCGA cases were separated into two groups and dichotomized into low (n = 89) and high (n = 104) S100A8/A9 cohorts as above. mRNA expression levels of VEGF-A/C and NGF were significantly greater in S100A8/A9-high than -low HNSCC tumors. EGFR mRNA expression was similar in S100A8/A9-high and -low neoplasms. Data shown as Mean (log_{10}) ± SEM; **p = 0.008, *p = 0.02 (two-tailed Student's *t*-test with equal variance). RPM: Reads per million.

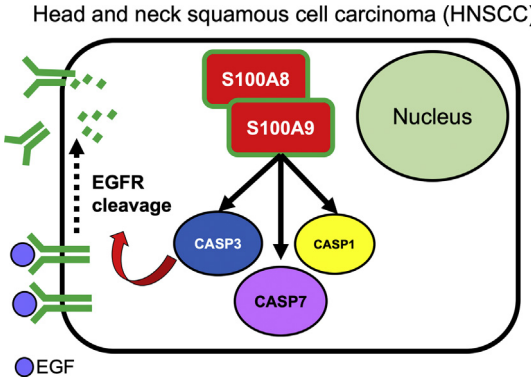

Fig. 5. Proposed protective mechanism of S100A8/A9-driven caspase-mediated EGFR cleavage in HNSCC. Caspases 1, 3 and 7 can proteolytically cleave and post-translationally modify EGFR [20,21]. When expressed in HNSCC tumors, calprotectin is hypothesized to increase the transcriptional levels and activity of caspases 1, 3, and 7, thus leading to post-translational proteolytic cleavage of membranous EGFR at the C-terminus. S100A8/A9-associated downregulation of EGFR could potentially contribute to the increased overall survival rates of patients with S100A8/A9-high HNSCC.

expression (expression score ≤ 9). Approximately 12% of PEDs of the oral cavity are estimated to progress into invasive carcinomas [39]. Whether risk of malignant transformation is higher in S100A8/A9-low PED than S100A8/A9-high precancerous lesions is not known.

Intraepithelial cell S100A8 and S100A9 protein levels appear lower in oral inflammatory and leukoplakic lesions than apparently normal mucosal epithelium [44]. Using gene network analyses, S100A8/A9 appears to contribute to downregulation of expression of invasion- and tumorigenesis-associated genes including *MMP1* and *INHBA* [10]. Hence, loss of calprotectin in a subset of dysplastic epithelial cells may accelerate cell proliferation and induce expression of cancer-promoting genes to initiate HNSCC. Upon release from polymorphonuclear neutrophils, macrophages and damaged epithelial cells, however, *extracellular* calprotectin is an "alarmin", signaling a pro-inflammatory response through toll-like receptor 4 (TLR4) and receptor for advanced glycation end products (RAGE) [40,41]. S100A8/A9 engagement by membrane receptors activates downstream cellular pathways, including mitogen-activated protein kinases (MAPK), Cdc42/Rac, and nuclear factor κB (NFκB) [42,43]. How these separate functions of S100A8/A9 intersect during tumorigenesis is a subject for future study.

Interestingly, *S100A8* and *S100A9* dysregulation is similar across all tumor grades (T) and is independent of nodal involvement (N) or distant metastasis (M) [10] but related to loco-regional recurrence [45]. S100A8/A9 is downregulated in oral, oropharyngeal, esophageal, nasopharyngeal, and cervical carcinomas [10–12,46,47]. In contrast, calprotectin expression appears induced in malignant neoplasms arising in the skin [48], breast [49–51], thyroid [52], liver [53], gastric mucosa [40], prostate [43], ovary [54], urinary bladder [55] and lung [56]. Within human tumor cells, therefore, regulation and expression of S100A8/A9 appear to be cell lineage- and tissue type-dependent.

In breast, prostate, colorectal and thyroid carcinomas, and melanoma, calprotectin is upregulated in the primary tumors and/or inflammatory cells and appears to promote metastatic spread [57]. Since calprotectin is downregulated in primary HNSCC, we also determined whether levels were further decreased in metastatic tumors by studying paired primary HNSCC and cervical lymph node metastases. The metastatic foci are more anaplastic than their primary counterparts. Since calprotectin expression is directly related to epithelial differentiation in HNSCC, we anticipated lower S100A8 and S100A9 levels in the metastatic lesions. In the 11-paired metastatic nodal tumors, calprotectin expression tended to be lower than the primary tumors but the decrease was not significant.

Mechanisms underlying metastasis are complex and include phenotypic plasticity of tumor cells and intrinsic genetic alterations favoring a stem cell-like state [58]. Interestingly, S100A8/A9 expression appears dichotomous across individuals with HNSCC, particularly grade II (MD) and III (PD) tumors, suggesting the tautochronous presence of two cancer cell populations. One subpopulation contains S100A8/A9-high, better differentiated and slowly-proliferating neoplastic cells. The second consists of S100A8/A9-low, less differentiated or anaplastic cells with higher proliferative and mitotic activity, increased migratory and invasive potential, and higher tumor-forming properties as we reported [9,10,17]. We predict, therefore, that pre-metastatic niches and distant metastases more readily form from S100A8/A9-low or -negative HNSCC than S100A8/A9-high and plan to test this prediction.

Independent of tobacco and alcohol usage, HNSCC tumorigenesis is increasingly associated with HPV infection [59,60]. Based on TCGA data, *S100A8* and *S100A9* expression tended to decrease more (non-significant) in HPV-positive than in HPV-negative HNSCC [10]. Among the 46 HNSCC specimens we investigated for S100A8/A9 IHC positivity, only a small fraction (13%) were considered positive for transcriptionally active HPV infection based on expression of the surrogate

marker, p16. All p16-positive tumors were histopathologically non-keratinizing or basaloid. Interestingly, NK/BAS HNSCCs were consistently S100A8- and S100A9-negative. When compared to HPV-negative oral PEDs, HPV-positive (koilocytic) dysplasias showed significantly less S100A8 and S100A9 (data not shown). In HPV-infected epithelial cells, calprotectin may inhibit viral oncogenic activity by regulating CKII-mediated E7 phosphorylation [61].

S100A8 and *S100A9* do not appear to be the only members of the EDC regulated by HPV. The cornified cell envelope proteins involucrin (*IVL*) and loricrin (*LOR*) are transcriptionally downregulated by E6 and E7 HPV oncoproteins in proliferating and differentiating human foreskin keratinocytes [62,63]. Specifically, involucrin is indirectly suppressed by E6 oncoprotein through HPV-mediated downregulation of transcription factor C/EBPα [64]. Given that C/EBPα, which regulates cellular growth and differentiation, appears to be essential for *S100A8* and *S100A9* expression [65,66], we speculate that an HPV-driven decrease in C/EBPα is responsible for S100A8/A9 downregulation seen in HPV (+) dysplastic and carcinomatous lesions. Since calprotectin appears to function as a tumor suppressor in HNSCC, HPV-induced, indirect downregulation of S100A8/A9 may represent an additional tumorigenic mechanism.

In some human malignancies, cancer progression is also influenced by VEGF-A-mediated vascularization [25,26] and VEGF-C-associated lymphangiogenesis, early spread, and metastasis to lymph nodes [27,28]. NGF and its primary receptor TrKA are associated with spread of HNSCC [23,24]. Yet, we found that VEGF-A /C and NGF protein expression appeared unaffected by calprotectin status *in vitro* and *ex vivo*. Based upon TCGA data, which includes tumor-infiltrating lymphoid cells, *VEGF-A/C* and *NGF* mRNA expression was greater in S100A8/A9-high than -low HNSCC. In the absence of the tumor microenvironment, however, VEGF-A/C and NGF expression appear independent of S100A8/A9 in TR146 cells. Although the VEGF-A/C and NGF responses may be idiosyncratic to TR146 cells and S100A8/A9 silencing, in the tumor milieu expression levels would reflect non-carcinoma stromal and inflammatory cells.

In summary, intracellular S100A8 and S100A9 (calprotectin) expression appears decreased or lost during the progression of HNSCC. Loss is not likely to be explained by release into the tumor stroma. The stroma does not stain positively; release of calprotectin is generally associated with apoptotic or necrotic cells. S100A8/A9 appears to be directly associated with the level of squamous differentiation and keratinization in HNSCC and inversely correlated with EGFR. S100A8/A9 appears to drive EGFR cleavage in a caspase-3/7–dependent pathway. Thus, S100A8/A9-associated downregulation of EGFR could contribute to the increased overall survival rates of patients with S100A8/A9-high HNSCC. These data further support the role of the calprotectin complex as a tumor-suppressive mechanism in HNSCC [11] and suggest targets for new therapeutic strategies.

Declaration of Competing Interest

The authors have no financial or other conflicts of interest with the publication of this work.

Acknowledgements

The project was supported by NIH/NIDCR R01DE021206 to MCH and R90DE023058 to PPA. We thank Rachel Isaksson Vogel, PhD for assistance with our statistical analyses. The content is solely the responsibility of the authors and does not necessarily represent the official views of the NIDCR or the NIH.

Appendix A. Supplementary material

Supplementary data to this article can be found online at https://doi.org/10.1016/j.oraloncology.2019.05.027.

References

[1] Cai Y, Dodhia S, Su GH. Dysregulations in the PI3K pathway and targeted therapies for head and neck squamous cell carcinoma. Oncotarget 2017;8:22203–17.
[2] Ferlay J, Shin HR, Bray F, Forman D, Mathers C, Parkin DM. Estimates of worldwide burden of cancer in 2008: GLOBOCAN 2008. Int J Cancer 2010;127:2893–917.
[3] Sivasithamparam J, Visk CA, Cohen EE, King AC. Modifiable risk behaviors in patients with head and neck cancer. Cancer 2013;119:2419–26.
[4] D'Souza G, Kreimer AR, Viscidi R, Pawlita M, Fakhry C, Koch WM, et al. Case-control study of human papillomavirus and oropharyngeal cancer. N Engl J Med 2007;356:1944–56.
[5] Miller KD, Siegel RL, Lin CC, Mariotto AB, Kramer JL, Rowland JH, et al. Cancer treatment and survivorship statistics, 2016. CA Cancer J Clin 2016;66:271–89.
[6] Warnakulasuriya S. Global epidemiology of oral and oropharyngeal cancer. Oral Oncol 2009;45:309–16.
[7] Leukert N, Sorg C, Roth J. Molecular basis of the complex formation between the two calcium-binding proteins S100A8 (MRP8) and S100A9 (MRP14). Biol Chem 2005;386:429–34.
[8] Nacken W, Roth J, Sorg C, Kerkhoff C. S100A9/S100A8: Myeloid representatives of the S100 protein family as prominent players in innate immunity. Microsc Res Technol 2003;60:569–80.
[9] Khammanivong A, Wang C, Sorenson BS, Ross KF, Herzberg MC. S100A8/A9 (calprotectin) negatively regulates G2/M cell cycle progression and growth of squamous cell carcinoma. PLoS ONE 2013;8:e69395.
[10] Khammanivong A, Sorenson BS, Ross KF, Dickerson EB, Hasina R, Lingen MW, et al. Involvement of calprotectin (S100A8/A9) in molecular pathways associated with HNSCC. Oncotarget 2016;7:14029–47.
[11] Argyris PP, Slama ZM, Ross KF, Khammanivong A, Herzberg MC. Calprotectin and the Initiation and Progression of Head and Neck Cancer. J Dent Res 2018;97:674–82.
[12] Funk S, Mark R, Bayo P, Flechtenmacher C, Grabe N, Angel P, et al. High S100A8 and S100A12 protein expression is a favorable prognostic factor for survival of oropharyngeal squamous cell carcinoma. Int J Cancer 2015;136:2037–46.
[13] Nisapakultorn K, Ross KF, Herzberg MC. Calprotectin expression in vitro by oral epithelial cells confers resistance to infection by Porphyromonas gingivalis. Infect Immun 2001;69:4242–7.
[14] Zaia AA, Sappington KJ, Nisapakultorn K, Chazin WJ, Dietrich EA, Ross KF, et al. Subversion of antimicrobial calprotectin (S100A8/S100A9 complex) in the cytoplasm of TR146 epithelial cells after invasion by Listeria monocytogenes. Mucosal Immunol 2009;2:43–53.
[15] Bhattacharya S, Bunick CG, Chazin WJ. Target selectivity in EF-hand calcium binding proteins. Biochim Biophys Acta, Rev Cancer 2004;1742:69–79.
[16] Hsu K, Champaiboon C, Guenther BD, Sorenson BS, Khammanivong A, Ross KF, et al. Anti-infective protective properties of S100 calgranulins. Antiinflamm Antiallergy Agents Med Chem 2009;8:290–305.
[17] Silva EJ, Argyris PP, Zou X, Ross KF, Herzberg MC. S100A8/A9 regulates MMP-2 expression and invasion and migration by carcinoma cells. Int J Biochem Cell Biol 2014;55:279–87.
[18] Mitsudomi T, Yatabe Y. Epidermal growth factor receptor in relation to tumor development: EGFR gene and cancer. FEBS J 2010;277:301–8.
[19] Arteaga CL, Engelman JA. ERBB receptors: from oncogene discovery to basic science to mechanism-based cancer therapeutics. Cancer Cell 2014;25:282–303.
[20] Bae SS, Choi JH, Oh YS, Perry DK, Ryu SH, Suh PG. Proteolytic cleavage of epidermal growth factor receptor by caspases. FEBS Lett 2001;491:16–20.
[21] He YY, Huang JL, Chignell CF. Cleavage of epidermal growth factor receptor by caspase during apoptosis is independent of its internalization. Oncogene 2006;25:1521–31.
[22] Mancino M, Ametller E, Gascón P, Almendro V. The neuronal influence on tumor progression. Biochim Biophys Acta, Rev Cancer 2011;1816:105–18.
[23] Bakst RL, Wong RJ. Mechanisms of Perineural Invasion. J Neurol Surg B Skull Base 2016;77:96–106.
[24] Roh J, Muelleman T, Tawfik O, Thomas SM. Perineural growth in head and neck squamous cell carcinoma: a review. Oral Oncol 2015;51:16–23.
[25] Ellis LM, Hicklin DJ. Pathways mediating resistance to vascular endothelial growth factor-targeted therapy. Clin Cancer Res 2008;14:6371–5.
[26] Ellis LM, Hicklin DJ. VEGF-targeted therapy: mechanisms of anti-tumour activity. Nat Rev Cancer 2008;8:579–91.
[27] Orellana C. Is lymphangiogenesis as important as angiogenesis? Lancet Oncol 2005;6:265.
[28] Achen MG, Stacker SA. Tumor lymphangiogenesis and metastatic spread-new players begin to emerge. Int J Cancer 2006;119:1755–60.
[29] Sorenson BS, Khammanivong A, Guenther BD, Ross KF, Herzberg MC. IL-1 receptor regulates S100A8/A9-dependent keratinocyte resistance to bacterial invasion. Mucosal Immunol 2012;5:66–75.
[30] Dickson MA, Hahn WC, Ino Y, Ronfard V, Wu JY, Weinberg RA, et al. Human keratinocytes that express hTERT and also bypass a p16(INK4a)-enforced mechanism that limits life span become immortal yet retain normal growth and differentiation characteristics. Mol Cell Biol 2000;20:1436–47.
[31] Giacaman RA, Nobbs AH, Ross KF, Herzberg MC. Porphyromonas gingivalis selectively up-regulates the HIV-1 coreceptor CCR5 in oral keratinocytes. J Immunol 2007;179:2542–50.
[32] Vacharaksa A, Asrani AC, Gebhard KH, Fasching CE, Giacaman RA, Janoff EN, et al. Oral keratinocytes support non-replicative infection and transfer of harbored HIV-1 to permissive cells. Retrovirology 2008;5:66.
[33] Ghavami S, Eshragi M, Ande SR, Chazin WJ, Klonisch T, Halayko AJ, et al. S100A8/

A9 induces autophagy and apoptosis via ROS-mediated cross-talk between mitochondria and lysosomes that involves BNIP3. Cell Res 2010;20:314–31.
[34] Nakatani Y, Yamazaki M, Chazin WJ, Yui S. Regulation of S100A8/A9 (calprotectin) binding to tumor cells by zinc ion and its implication for apoptosis-inducing activity. Mediators Inflamm 2005;2005:280–92.
[35] Zhuang S, Ouedraogo GD, Kochevar IE. Downregulation of epidermal growth factor receptor signaling by singlet oxygen through activation of caspase-3 and protein phosphatases. Oncogene 2003;22:4413–24.
[36] Roesch Ely M, Nees M, Karsai S, Mägele I, Bogumil R, Vorderwülbecke S, et al. Transcript and proteome analysis reveals reduced expression of calgranulins in head and neck squamous cell carcinoma. Eur J Cell Biol 2005;84:431–44.
[37] Sapkota D, Bruland O, Bøe OE, Bakeer H, Elgindi OA, Vasstrand EN, et al. Expression profile of the S100 gene family members in oral squamous cell carcinomas. J Oral Pathol Med 2008;37:607–15.
[38] Reckenbeil J, Kraus D, Probstmeier R, Allam JP, Novak N, Frentzen M, et al. Cellular distribution and gene expression pattern of metastasin (S100A4), calgranulin A (S100A8), and calgranulin B (S100A9) in oral lesions as markers for molecular pathology. Cancer Invest 2016;34:246–54.
[39] Mehanna HM, Rattay T, Smith J, McConkey CC. Treatment and follow-up of oral dysplasia - a systematic review and meta-analysis. Head Neck 2009;31:1600–9.
[40] Turovskaya O, Foell D, Sinha P, Vogl T, Newlin R, Nayak J, et al. RAGE, carboxylated glycans and S100A8/A9 play essential roles in colitis-associated carcinogenesis. Carcinogenesis 2008;29:2035–43.
[41] Källberg E, Vogl T, Liberg D, Olsson A, Björk P, Wikström P, et al. S100A9 interaction with TLR4 promotes tumor growth. PLoS ONE 2012;7:e34207.
[42] Schmidt AM, Hofmann M, Taguchi A, Yan SD, Stern DM. RAGE: a multiligand receptor contributing to the cellular response in diabetic vasculopathy and inflammation. Semin Thromb Hemost 2000;26:485–93.
[43] Hermani A, De Servi B, Medunjanin S, Tessier PA, Mayer D. S100A8 and S100A9 activate MAP kinase and NF-kappaB signaling pathways and trigger translocation of RAGE in human prostate cancer cells. Exp Cell Res 2006;312:184–97.
[44] Driemel O, Murzik U, Escher N, Melle C, Bleul A, Dahse R, et al. Protein profiling of oral brush biopsies: S100A8 and S100A9 can differentiate between normal, premalignant, and tumor cells. Proteomics Clin Appl 2007;1:486–93.
[45] Harris TM, Du P, Kawachi N, Belbin TJ, Wang Y, Schlecht NF, et al. Proteomic analysis of oral cavity squamous cell carcinoma specimens identifies patient outcome-associated proteins. Arch Pathol Lab Med 2015;139:494–507.
[46] Gonzalez HE, Gujrati M, Frederick M, Henderson Y, Arumugam J, Spring PW, et al. Identification of 9 genes differentially expressed in head and neck squamous cell carcinoma. Arch Otolaryngol Head Neck Surg 2003;129:754–9.
[47] Kong JP, Ding F, Zhou CN, Wang XQ, Miao XP, Wu M, et al. Loss of myeloid-related proteins 8 and myeloid-related proteins 14 expression in human esophageal squamous cell carcinoma correlates with poor differentiation. World J Gastroenterol 2004;10:1093–7.
[48] Gebhardt C, Németh J, Angel P, Hess J. S100A8 and S100A9 in inflammation and cancer. Biochem Pharmacol 2006;72:1622–31.
[49] Arai K, Takano S, Teratani T, Ito Y, Yamada T, Nozawa R. S100A8 and S100A9 overexpression is associated with poor pathological parameters in invasive ductal carcinoma of the breast. Curr Cancer Drug Targets 2008;8:243–52.
[50] Moon A, Yong HY, Song JI, Cukovic D, Salagrama S, Kaplan D, et al. Global gene expression profiling unveils S100A8/A9 as candidate markers in H-ras-mediated human breast epithelial cell invasion. Mol Cancer Res 2008;6:1544–53.
[51] Rodriguez-Barrueco R, Yu J, Saucedo-Cuevas LP, Olivan M, Llobet-Navas D, Putcha P, et al. Inhibition of the autocrine IL-6-JAK2-STAT3-calprotectin axis as targeted therapy for HR-/HER2+ breast cancers. Genes Dev 2015;29:1631–48.
[52] Ito Y, Arai K, Nozawa R, Yoshida H, Hirokawa M, Fukushima M, et al. S100A8 and S100A9 expression is a crucial factor for dedifferentiation in thyroid carcinoma. Anticancer Res 2009;29:4157–61.
[53] Németh J, Stein I, Haag D, Riehl A, Longerich T, Horwitz E, et al. S100A8 and S100A9 are novel nuclear factor kappa B target genes during malignant progression of murine and human liver carcinogenesis. Hepatology 2009;50:1251–62.
[54] Ødegaard E, Davidson B, Elgaaen BV, Fagerhol MK, Engh V, Onsrud M, et al. Circulating calprotectin in ovarian carcinomas and borderline tumors of the ovary. Am J Obstet Gynecol 2008;198(418):e1–7.
[55] Yao R, Davidson DD, Lopez-Beltran A, MacLennan GT, Montironi R, Cheng L. The S100 proteins for screening and prognostic grading of bladder cancer. Histol Histopathol 2007;22:1025–32.
[56] Kawai H, Minamiya Y, Takahashi N. Prognostic impact of S100A9 overexpression in non-small cell lung cancer. Tumour Biol 2011;32:641–6.
[57] Bresnick AR, Weber DJ, Zimmer DB. S100 proteins in cancer. Nat Rev Cancer 2015;15:96–109.
[58] Brabletz T. To differentiate or not–routes towards metastasis. Nat Rev Cancer 2012;12:425–36.
[59] Thibaudeau E, Fortin B, Coutlée F, Nguyen-Tan P, Weng X, Audet ML, et al. HPV prevalence and prognostic value in a prospective cohort of 255 patients with locally advanced HNSCC: a single-centre experience. Int J Otolaryngol 2013;2013:437815.
[60] Dayyani F, Etzel CJ, Liu M, Ho CH, Lippman SM, Tsao AS. Meta-analysis of the impact of human papillomavirus (HPV) on cancer risk and overall survival in head and neck squamous cell carcinomas (HNSCC). Head Neck Oncol 2010;2:15.
[61] Tugizov S, Berline J, Herrera R, Penaranda ME, Nakagawa M, Palefsky J. Inhibition of human papillomavirus type 16 E7 phosphorylation by the S100 MRP-8/14 protein complex. J Virol 2005;79:1099–112.
[62] Lehr E, Brown DR. Infection with the oncogenic human papillomavirus type 59 alters protein components of the cornified cell envelope. Virology 2003;309:53–60.
[63] Gyöngyösi E, Szalmás A, Ferenczi A, Kónya J, Gergely L, Veress G. Effects of human papillomavirus (HPV) type 16 oncoproteins on the expression of involucrin in human keratinocytes. Virol J 2012;9:36.
[64] Marthaler AM, Podgorska M, Feld P, Fingerle A, Knerr-Rupp K, Grässer F, et al. Identification of C/EBPα as a novel target of the HPV8 E6 protein regulating miR-203 in human keratinocytes. PLoS Pathog 2017;13:e1006406.
[65] Cammenga J, Mulloy JC, Berguido FJ, MacGrogan D, Viale A, Nimer SD. Induction of C/EBPalpha activity alters gene expression and differentiation of human CD34+ cells. Blood 2003;101:2206–14.
[66] Tavor S, Park DJ, Gery S, Vuong PT, Gombart AF, Koeffler HP. Restoration of C/EBPalpha expression in a BCR-ABL+ cell line induces terminal granulocytic differentiation. J Biol Chem 2003;278:52651–9.